Mechanistic Investigation of the Ruthenium-N-Heterocyclic-Carbene-Catalyzed Amidation of Amines with Alcohols

ARTICLE *in* CHEMISTRY - A EUROPEAN JOURNAL · DECEMBER 2012

Impact Factor: 5.73 · DOI: 10.1002/chem.201202400 · Source: PubMed

3 AUTHORS, INCLUDING:

Peter Fristrup
Technical University of Denmark
60 PUBLICATIONS **1,174** CITATIONS

SEE PROFILE

DOI: 10.1002/chem.201202400

Mechanistic Investigation of the Ruthenium–N-Heterocyclic-Carbene-Catalyzed Amidation of Amines with Alcohols

Ilya S. Makarov, Peter Fristrup,* and Robert Madsen*[a]

Abstract: The mechanism of the ruthenium–N-heterocyclic-carbene-catalyzed formation of amides from alcohols and amines was investigated by experimental techniques (Hammett studies, kinetic isotope effects) and by a computational study with dispersion-corrected density functional theory (DFT/M06). The Hammett study indicated that a small positive charge builds-up at the benzylic position in the transition state of the turnover-limiting step. The kinetic isotope effect was determined to be 2.29(±0.15), which suggests that the breakage of the C–H bond is not the rate-limiting step, but that it is one of several slow steps in the catalytic cycle. Rapid scrambling of hydrogen and deuterium at the α position of the alcohol was observed with deuterium-labeled substrates, which implies that the catalytically active species is a ruthenium dihydride. The experimental results were supported by the characterization of a plausible catalytic cycle by using DFT/M06. Both *cis*-dihydride and *trans*-dihydride intermediates were considered, but when the theoretical turnover frequencies (TOFs) were derived directly from the calculated DFT/M06 energies, we found that only the *trans*-dihydride pathway was in agreement with the experimentally determined TOFs.

Keywords: amides · density functional calculations · isotope effect · reaction mechanisms · ruthenium

Introduction

The (carbox)amide group constitutes one of the most-significant functional groups in organic chemistry. The synthesis of amides is usually performed from carboxylic acids and amines by using a coupling reagent or by prior conversion of the acid into an activated derivative. Recently, however, several new and fundamentally different approaches to amide synthesis have been developed.[1] These emerging methods include the umpolung synthesis from α-bromonitroalkanes,[2] the decarboxylative condensation of α-ketoacids and hydroxylamines,[3] and the metal-catalyzed coupling of primary alcohols and amines.[4–6] This latter reaction can be carried out by aerobic oxidation with heterogeneous gold catalysts[4] or by dehydrogenation with various homogeneous and heterogeneous catalysts.[5,6] The dehydrogenative synthesis of amides from alcohols and amines can be performed both in the presence or absence of a hydrogen acceptor, such as a ketone or an alkene.[5,6] The most-attractive procedures would avoid the need for hydrogen scavengers altogether, which can be achieved with homogeneous ruthenium pincers,[5a] carbenes,[5b,c] and diamine–diphosphine[5d] complexes, as well as with heterogeneous Ag/Al_2O_3[5e] and Au/hydrotalcite catalysts.[5f] To further develop these amidation procedures, it is important to gain a better understanding of the underlying reaction mechanisms. So far, the umpolung approach with α-bromonitroalkanes and the decarboxylative pathway with α-ketoacids have been studied with ^{18}O-labeled substrates,[7] whilst the first step in the dehydrogenative reaction with ruthenium pincer complexes has been investigated by low-temperature NMR spectroscopy.[8] In addition, computational studies have been performed on the ruthenium-catalyzed transformations with pincer and diamine–diphosphine complexes.[9]

The amidation reaction between primary alcohols and amines catalyzed by ruthenium–N-heterocyclic-carbene complexes was first reported by our group in 2008;[5b] since then, this transformation has been further investigated with regard to catalyst precursors and substrate scope.[10] This reaction is most-effectively catalyzed by complex **1** (Figure 1) in the presence of PCy_3 and KO*t*Bu. No stoichiometric additives are necessary and the amidation reaction produces hydrogen gas as the only byproduct. The reaction is believed to proceed through dehydrogenation of the alcohol into the corresponding aldehyde, which stays coordinated to the ruthenium catalyst (Scheme 1). Then, nucleophilic attack by the amine forms the hemiaminal, which is dehydrogenated to afford the amide. The fact that the intermediate aldehyde remains coordinated to the ruthenium center is an important observation that has been confirmed experimentally by a cross-

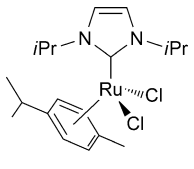

1

Figure 1. Structure of compound **1**.

[a] I. S. Makarov, Dr. P. Fristrup, Prof. Dr. R. Madsen
Department of Chemistry, Building 201
Technical University of Denmark, 2800 Kgs. Lyngby (Denmark)
Fax: (+45) 4593-3968
E-mail: pf@kemi.dtu.dk
rm@kemi.dtu.dk

Supporting information for this article is available on the WWW under http://dx.doi.org/10.1002/chem.201202400.

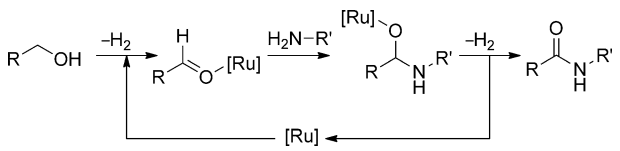

Scheme 1. Dehydrogenative synthesis of amides from alcohols and amines.

over experiment.[10e] However, the mechanism of the amidation reaction has not previously been subjected to a more-thorough examination.

Herein, we report a combined experimental and theoretical mechanistic investigation of the formation of amides from alcohols and amines catalyzed by ruthenium–N-heterocyclic-carbene complex **1**.

Results and Discussion

For the experimental study, the catalyst system was modified slightly to obtain more-accurate and reproducible results. Tricyclohexylphosphine is easily oxidized by air and commercial samples contain various amounts of impurities that are difficult to remove. To solve this problem, Netherton and Fu replaced trialkylphosphines with their corresponding HBF_4 salts in several metal-catalyzed reactions.[11] These salts are air-stable and the phosphine can be released into the reaction with a Brønsted base. Moreover, because a base is already required for the amidation reaction, we decided to replace PCy_3 with $PCy_3{\cdot}HBF_4$ and increase the amount of KO*t*Bu accordingly. This modification gave more-consistent results and, therefore, the experimental mechanistic study was performed on the following system: $[RuCl_2(I\mathit{i}Pr)(\mathit{p}\text{-cymene})]$ (5 mol%), $PCy_3{\cdot}HBF_4$ (5 mol%), and KO*t*Bu (15 mol%) in refluxing toluene.

Hammett study: We have previously used Hammett studies with *para*-substituted benzaldehydes to analyze the turnover-limiting step in several metal-mediated reactions.[12] This method makes it possible to determine the change in charge at the benzylic position between the starting material and the transition state. Subsequently, the development of charge can be simulated in silico, based on a proposed catalytic cycle, and can be used to discriminate between different mechanistic scenarios. In this case, the Hammett study will be comprised of a series of competition reactions between benzyl alcohol and various *para*-substituted benzyl alcohols with hexylamine as the amine component (Scheme 2). First, the amidation reactions of hexylamine with different *para*-substituted benzyl alcohols were carried out and the reaction was found to proceed cleanly and in high yield with both electron-donating and electron-withdrawing groups in the *para* position (Table 1).

Because the amidation reaction occurs with the negligible formation of byproducts, the course of the competition reactions could be followed by measuring the disappearance of the alcohols by using GC. Assuming that all of the substrates react according to the same mechanism and that the reaction is first order in the alcohol, their relative reactivities (k_X/k_H) can be obtained as the slope of the line when $\ln(c_0/c)$ for one *para*-substituted benzyl alcohol is plotted against the same values for benzyl alcohol. This plot resulted in good linear correlations for all six *para*-substituted benzyl alcohols (Figure 2), which confirmed the assumption that the amidation reaction was first order in the alcohol. In each case, the correlation coefficient was ≥ 0.99 and the benzyl alcohols with electron-donating *para* substituents reacted faster than alcohols with electron-withdrawing groups. The slopes could then be used to construct the Hammett plot based on σ values from the literature[13] (Figure 3). The best correlation was achieved with σ^+ values, which afforded a straight line with a small negative slope ($\rho = -0.15$). This result indicates that a small positive charge is build-up at the benzylic position in the transition state of the turnover-limiting step. The correlation with Creary's $\sigma^{\bullet}$ values was poor and, therefore, a radical intermediate is not involved in the amidation reaction. The oxidation of an alcohol into an amide is likely to proceed through two consecutive β-hydride eliminations, which result in the formation of an aldehyde and an amide, respectively. Either of these elimination steps are good candidates for the turnover-limiting step be-

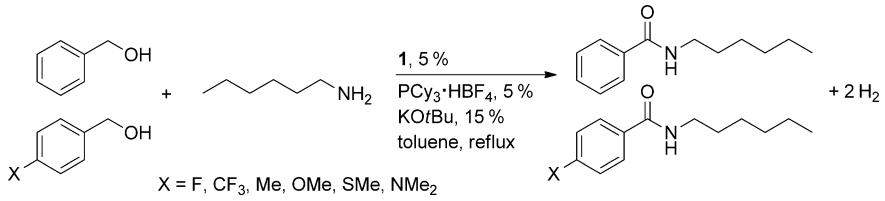

Scheme 2. Competition experiments for the amidation of benzyl alcohol versus that of *para*-substituted benzyl alcohols **2b**–**2g**.

Table 1. Amidation of *para*-substituted benzyl alcohols **2a**–**2g**.

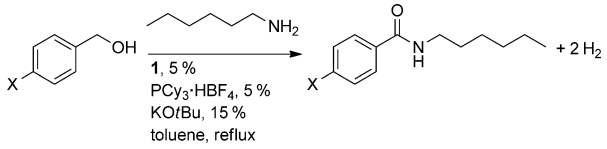

Entry	Compound	X	Yield [%][a]
1	**2a**	H	90
2	**2b**	CF_3	70
3	**2c**	F	80
4	**2d**	Me	94
5	**2e**	OMe	100
6	**2f**	SMe	88
7	**2g**	NMe_2	100

[a] Yield of isolated product after 24 h.

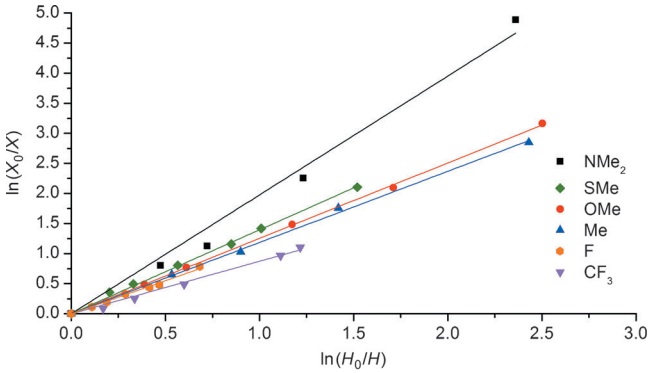

Figure 2. Kinetic data for the amidation of *para*-substituted benzyl alcohols **2b**–**2g** in competition with compound **2a** ("0" denotes initial concentration, X is the concentration of compounds **2b**–**2g**, and H is the concentration of compound **2a**).

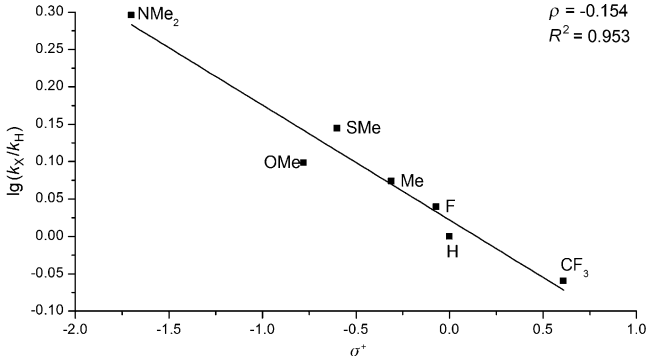

Figure 3. Hammett plot for the amidation of alcohols **2a**–**2g**.

cause, in both cases, a partial positive charge is formed at the benzylic position in the transition state.

Reaction order: To gain more information about the role of each component, we sought to determine the kinetic order in these constituents. First, the order in the amine was examined by varying the concentration of hexylamine from 0.2–0.5 M whilst keeping the concentration of benzyl alcohol (0.5 M) and the ruthenium catalyst (25 mM) constant. The initial rate of the reaction was determined for each concentration of amine and the rates were plotted against the amine concentrations to give a straight line, thus indicating a first-order dependence in the amine (Figure 4a).

The reaction order in phosphine was examined by varying the concentration of PCy_3 from 0–5 mM whilst keeping the concentrations of benzyl alcohol and hexylamine constant (0.2 M). A non-linear dependence was observed and an order of 0.5 in phosphine was derived from a double-logarithmic plot (Figure 4b). This reaction order will be further addressed in the computational study and used to pinpoint the role of phosphine in the reaction mechanism.

Attempts to establish the reaction order in the ruthenium catalyst were initially met with difficulties. At low catalyst loadings ($\leq$2% or 10 mM), the amidation either proceeded with a long initiation period or did not proceed at all, which

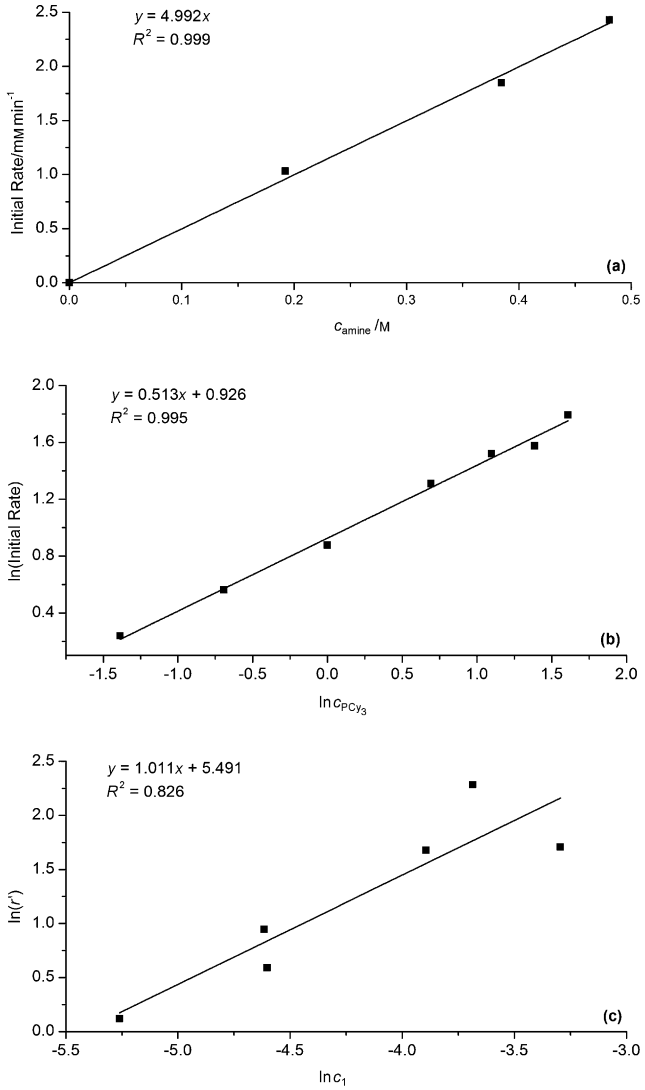

Figure 4. a) Plot of c_{amine} versus r_{init}; b) plot of $\ln c_{PCy_3}$ versus $\ln r_{init}$; c) Plot of $\ln c_1$ versus $\ln r'_{init}$.

made it impossible to obtain reproducible results. At higher loadings (>6%), the initial rate measurements were also accompanied by significant uncertainties. After some experimentation, we found that more-reproducible results could be obtained if complex **1** was treated with PCy_3·HBF_4 and KO*t*Bu in refluxing toluene for 45 min before the alcohol and the amine were added. With this modification, the concentration of compound **1** was varied from 5–37 mM, whilst the concentrations of benzyl alcohol and hexylamine were kept constant (0.5 M). These data resulted in a straight line, as shown in Figure 4c, thus indicating a first-order dependence on the ruthenium catalyst. The experiments in Figure 4a were repeated under these slightly modified conditions and the same linear dependence was observed, which illustrates that the overall kinetics of the reaction have not been altered. The minimum amount of ruthenium catalyst for complete conversion under these conditions was about 1%, where the complete amidation of hexylamine with 2-

phenylethanol was observed in 24 h. This result should be compared to 0.1 % loading with a ruthenium pincer complex[5a] and to 4–5 % loading with ruthenium–triazolylidine[5c] and diamine–diphosphine[5d] complexes.

Deuterium-labeled substrates: Initially, we planned to determine the kinetic isotope effect (KIE) by using competition experiments in a similar way to the Hammett study. [α,α-D_2]Benzyl alcohol would be allowed to compete with benzyl alcohol in a reaction with hexylamine and the KIE would be calculated by measuring the disappearance of the two alcohols, which would be separable by GC. However, we quickly discovered that this simple experiment was not feasible because a rapid scrambling of deuterium and hydrogen occurred at the α position of the alcohol under the amidation conditions. Accordingly, we decided to study this scrambling in more detail and, to exclude a possible side-reaction with benzylic radicals, these experiments were performed with 2-phenylethanol (**3**) as the alcohol substrate.

First, the source of the atom scrambling was determined (Table 2). The reaction between non-deuterated 2-phenylethanol and benzylamine was performed in [D_8]toluene and

Table 2. Experiments to determine the positions of the scrambled atoms.

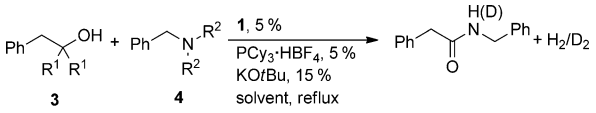

Entry	R^1	R^2	Solvent
1	H (**3**)	H (**4**)	[D_8]toluene
2	H (**3**)	D ([D_2]-**4**)	toluene
3	D ([D_2]-**3**)	H (**5**)	toluene

the relative amounts of non-deuterated, mono-deuterated, and di-deuterated alcohols were monitored by GCMS. This experiment showed no change in the deuterium content of the alcohol during the reaction, which demonstrates that no exchange with the solvent occurs (Figure 5, entry 1).

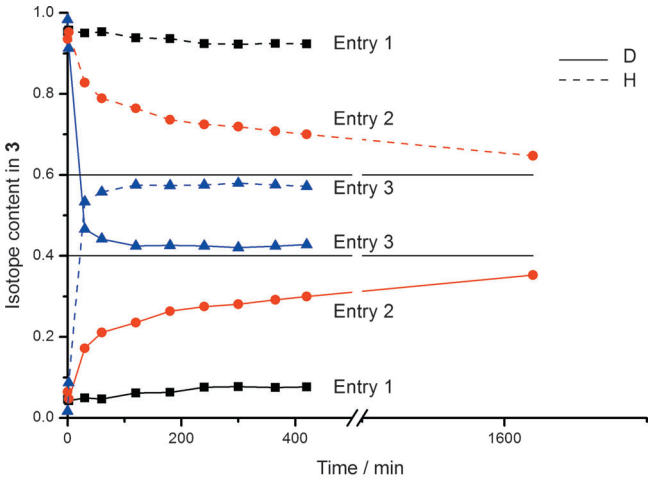

Figure 5. Experiments with deuterium-labeled substrates.

As a result, the exchangeable protons are most likely the two α protons on the primary alcohol, the O–H proton, and the two N–H protons in the primary amine. In a second experiment, non-deuterated 2-phenylethanol was reacted with $BnND_2$ and the deuterium content in the starting alcohol was monitored again as the reaction progressed (Figure 5, entry 2). This experiment showed that two hydrogen atoms in the alcohol were exchanged with deuterium and that the reaction must occur with the α protons because exchange of the O–H proton cannot be measured by GCMS. The scrambling occurred in such a fashion that an equilibrium was slowly reached at which the hydrogen/deuterium ratio for the two α protons was 3:2. This ratio is the same as that between the exchangeable hydrogen and deuterium atoms in the starting materials and confirms that all five protons take part in the scrambling. This result was verified by repeating the experiment with [D_2]-α,α-2-phenylethanol and non-deuterated benzylamine (Figure 5, entry 3). Again, equilibrium was reached at which the hydrogen/deuterium ratio for the two α protons in the alcohol was 3:2. However, in this case, the exchange occurred much more rapidly and was observed even before the amide had started to form. This result means that there is a reversible step at the beginning of the reaction, which most-likely involves a β-hydride elimination and a migratory insertion. More significantly, the scrambling implies that a ruthenium–dihydride species is involved in the catalytic cycle.

This result suggests that the two chloride ligands in complex **1** are not present in the catalytically active species, which, instead, is likely to be a ruthenium–dihydride species. To gain further support for this rationale, the two chloride atoms in complex **1** were replaced with a different halogen group. It has previously been shown that diiodide complexes [RuI_2(NHC)(*p*-cymene)] (NHC = IMe, I*i*Pr, and ICy) will also catalyze the amidation reaction,[10e,h] although the yields vary, possibly owing to the lower stabilities of these complexes. However, when we measured the initial rate with complex [RuI_2(I*i*Pr)(*p*-cymene)] under the standard conditions with benzyl alcohol and hexylamine, we obtained a value of 3.09 mM min^{-1}. This value is essentially the same as with complex **1** (3.37 mM min^{-1}), which strongly suggests that the halides are not bound to the ruthenium center in the catalytic cycle.

Kinetic isotope effect: With the knowledge of the deuterium scrambling and the atoms that are involved in this process in hand, we designed an experiment to determine the KIE of the overall reaction. First, the hydrogen atoms at the exchangeable positions in both the alcohol and the amine were replaced with deuterium and the initial rates for both the deuterated and non-deuterated substrates were then measured in two separate experiments. For convenience, commercially available and fully deuterated [D_{10}]-1-butanol was selected as the alcohol, whilst $BnND_2$ was chosen as the amine part. The initial rate with these deuterated substrates was 6.44(±0.02) mM min^{-1}, whilst the rate with non-deuterated 1-butanol and benzyl amine was 14.77(±0.96) mM min^{-1}.

These values gave an experimental KIE of 2.29(±0.15), which suggests that the breakage of the C–H bond is not the rate-limiting step, but instead is one of several slow steps in the catalytic cycle (see below).

NMR spectroscopy: The amidation reaction was also analyzed by NMR spectroscopy to identify possible intermediates during the transformation. First, we studied whether *p*-cymene stayed coordinated to the ruthenium center throughout the catalytic cycle. The reaction between compounds **3** and **4** was performed in [D_8]toluene at 110 °C with 15 mol % of compound **1** and with PPh_3 instead of PCy_3·HBF_4 to avoid the presence of additional signals in the aliphatic region of the spectrum. Samples were removed from the reaction mixture and analyzed at ambient temperature. We found that, after only 3 min, 85 % of *p*-cymene was in the solution in its unbound form and, after 10 min, *p*-cymene had completely decoordinated from the ruthenium atom.

Then, the reaction between 2-phenylethanol and benzylamine was monitored in [D_8]toluene with the NMR probe temperature set at 70 °C. A rather high catalyst loading was employed in this experiment with 40 % of compound **1**, 40 % of PCy_3·HBF_4, and 120 % of KO*t*Bu. During the reaction, several clusters of signals were detected in the hydride region of the spectrum. After 3 h, this cluster included low-intensity signals at $\delta = -7.44$ and -7.54 ppm, very low-intensity signals in the range $\delta = -10.66$ to -11.13 ppm, high-intensity doublets from $\delta = -17.41$ to -17.89 ppm (J(P,H) $\approx$ 20 Hz), as well as a high-intensity doublet at $\delta = -18.04$ ppm (J(H,H) = 7.1 Hz). These observations clearly reveal that several hydride species are formed during the amidation reaction.[10h] Moreover, the doublet at $\delta = -18.04$ ppm shows that there is a dihydride species that does not contain a phosphine group. The doublets from $\delta = -17.41$ to -17.89 ppm and their coupling constants suggest the presence of ruthenium–hydride complexes in which one phosphine group is coordinated *cis* to the hydride atom. Over time, the intensity of the signals decreased and some of them disappeared.

To study the reaction under conditions that were more similar to the actual setup, the amidation reaction was repeated in refluxing [D_8]toluene with a catalyst loading of 20 %. After 30 min, a sample was withdrawn and analyzed by ^{1}H and ^{31}P NMR spectroscopy at room temperature. In the ^{1}H NMR spectrum, several additional signals as well as the signals given above were observed in the hydride region, including a singlet at $\delta = -9.70$ ppm, a doublet at -15.04 ppm (J(P,H) = 22.5 Hz), and signals at $\delta \approx -17.8$ ppm. The presence of these signals also suggests the formation of several complexes in which the phosphine is *cis* to the hydride atom, as well as a complex without phosphine. The ^{31}P NMR spectrum reveals a group of signals in the range $\delta = 46$–51 ppm, a low-intensity signal at $\delta = 57.2$ ppm, and a high-intensity signal at $\delta = 10$ ppm. This latter signal is from free PCy_3, whereas the others may be assigned to ruthenium intermediates that contain coordinated phosphine. Therefore, these spectroscopic data provide further support for the formation of mono- and dihydride–ruthenium species during the reaction. In addition, the NMR spectroscopy experiments have demonstrated that complexes both with and without phosphine are present in the reaction mixture.

Computational study: To increase our understanding of the reaction pathway, our investigation was extended by performing a computational study, in line with earlier work.[12] A simplified system was chosen in which ethylamine and benzyl alcohol were used as reactants and 1,3-diisopropylimidazol-2-ylidene (I*i*Pr) and PCy_3 were coordinated to the ruthenium atom. All of these calculations were performed by using the M06 functional, which includes non-bonding interactions (not the case with DFT/B3LYP). In all of these calculations, the total energy (ΔG_{tot}) was represented by a combination of gas-phase energy (E_{scf}), solution-phase energy (E_{solv}), and Gibbs free energy (ΔG), as shown in [Eq. (1)]. This approach was first suggested by Wertz[14] and has later been applied in several studies of transition-metal-catalyzed reactions.[12a,b,15] This procedure avoids the time-consuming and error-prone calculation of numerical frequencies in the solution phase.

$$\Delta G_{tot} = \Delta G - E_{scf} + E_{solv} \quad (1)$$

First, we were interested in identifying the ligands that could be coordinated to the ruthenium center during the catalytic cycle. The precursor complex (**1**) is an 18-electron ruthenium(II) species, which loses *p*-cymene during the initiation step. Another possible ligand is the amine moiety, which is present in stoichiometric amounts. The DFT calculations show that the coordination of one molecule of amine is very favorable, with a decrease in ΔG_{tot} from -31 to -107 kJ mol^{-1}, depending on the other ligands on the ruthenium atom. This result strongly implies that an amine is bound to the metal center throughout the reaction. However, the coordination of a second molecule of amine at the apical position of the complex is less favorable than the coordination of a phosphine at this position (ΔG_{tot} increases from 6 to 40 kJ mol^{-1}, depending on the other ligands on ruthenium atom).

A detailed study of the initiation of the reaction is beyond the scope of this investigation. However, for similar ruthenium(II)–dichloride complexes, it has been established that, in the presence of alcohols, the chloride ligands can be replaced with alkoxide and hydride groups.[16] Thus, because the experimental study indicates that both chloride anions are replaced by other ligands, we decided to use 16-electron complex **5**, in which a hydride and an alkoxide ligand are coordinated to the ruthenium atom, as a starting point.

Our calculations show that complex **5** adopts a distorted octahedral orientation in which the two bulky ligands (I*i*Pr and phosphine) are in the apical positions and the amine, alkoxide, and hydride groups occupy the equatorial positions (Scheme 3). The alkoxide group must have an adjacent

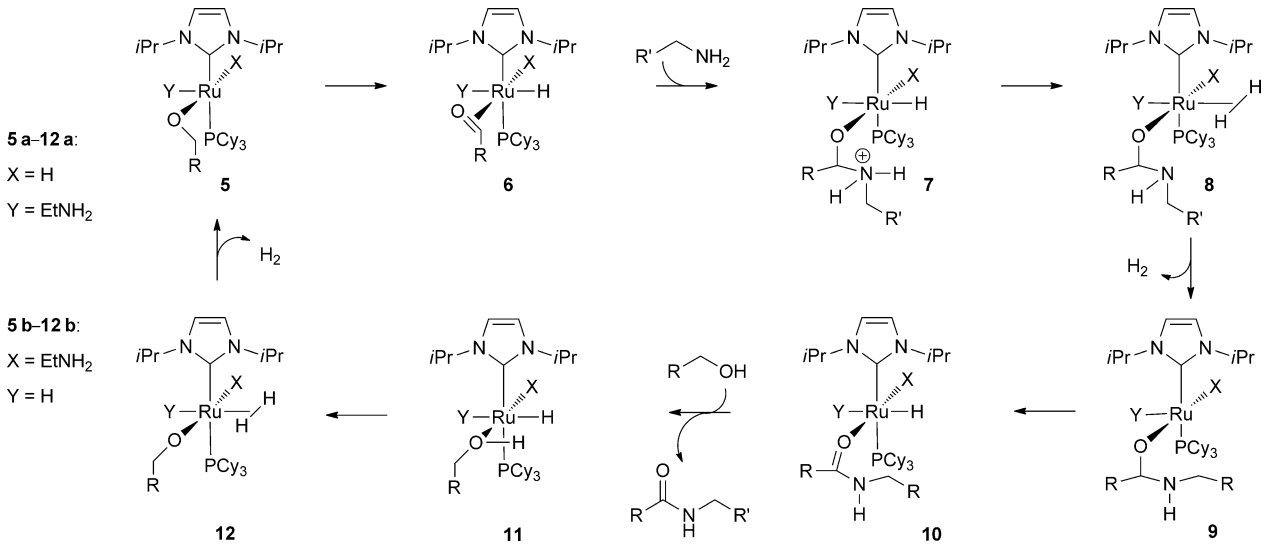

Scheme 3. Proposed catalytic cycle (**a**: *cis*-dihydride pathway; **b**: *trans*-dihydride pathway).

empty site for β-hydride elimination to occur. As a consequence, the amine and hydride groups can be positioned in two different ways and, thus, form two isomers (**5a** and **5b**). Either of these isomers can serve as an entry point into the catalytic cycle.

Interestingly, these two isomers, compounds **5a** and **5b**, have almost the same energy ($\Delta\Delta G_{tot}$(**5a**–**5b**) = 5.8 kJ mol^{-1}), which means that they can both be formed at the beginning of the reaction. To distinguish between these two possible pathways for the reaction, the entire catalytic cycles starting from either isomer **5a** or isomer **5b** were calculated. We expected that, by direct comparison between their experimental results and their calculated energy profiles, it would be possible to reach a conclusion about the orientation of the ligands. From the experiments with the deuterated substrates, it is known that deuterium scrambling takes place before the formation of the amide and that the rate of exchange is much higher than the rate of the amide-forming reaction. Most likely, the deuterium exchange occurs in the first β-hydride-elimination step when a dihydride species (**6**) is formed. The calculations show that the formation of species **6a** is exothermic, whereas the formation of species **6b** is endothermic (Figure 6). In addition, the activation energy for the reverse reaction is lower in the case of species **6b** ($\Delta\Delta E_a$(**6b**–**6a**) = −30.4 kJ mol^{-1}), whilst the difference in energy between the two transition states (**TS2** and **TS1**) is lower with species **6a** (ΔE_a(**TS2b**–**TS1b**) = 48.9 kJ mol^{-1}, ΔE_a(**TS2a**–**TS1a**) = 18.5 kJ mol^{-1}). These facts suggest that the observed β-hydride elimination is more plausible in the case of isomer **6b** than with isomer **6a**. Consequently, the noted equilibrium between deuterated and non-deuterated substrates will be determined by the **b** pathway in the first β-hydride-elimination step.

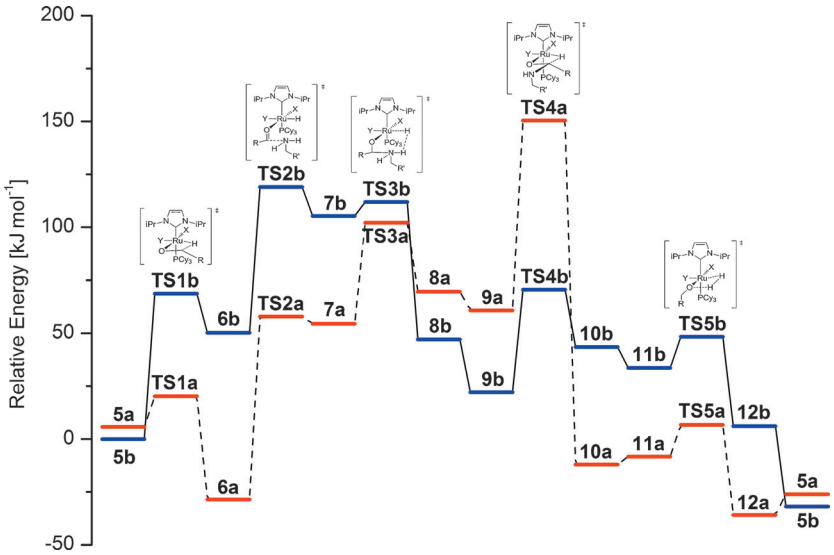

Figure 6. Energy profiles for the two possible catalytic cycles (**TS1a**–**TS5a**: X = H, Y = EtNH$_2$; **TS1b**–**TS5b**: X = EtNH$_2$, Y = H).

To gain additional support for the **b** route, the two pathways were compared quantitatively by calculating the turnover frequencies (TOFs) with the energetic span model. The concept of energetic span was introduced by Amatore and Jutand[17] and further developed by Kozuch and Shaik.[18]

This model replaces the classical Curtin–Hammett principle of the rate-limiting step in the catalytic cycle with the rate-limiting states, that is, the TOF-determining transition

state (TDTS) and the TOF-determining intermediate (TDI). The AUTOF program[19] was used to calculate the TOFs from the computationally obtained energy states. These calculations show that, for the **a** pathway, **TS4a** is the TDTS and species **6a** is the TDI, whereas, for the **b** pathway, **TS2b** is the TDTS and species **5b** is the TDI. In other words, the rate of the reaction is defined by the difference in energy (energetic span) between species **6a** and **TS4a** ($\Delta E = 189.1\ kJ\,mol^{-1}$) for the **a** pathway and between species **5b** and **TS2b** for the **b** pathway ($\Delta E = 119.0\ kJ\,mol^{-1}$). As a result of the large differences in energetic span between the two pathways, the calculated TOF for the catalytic cycle that proceeds through the **a** pathway is $1.04\times10^{-8}\ h^{-1}$, whereas the TOF for the catalytic cycle that proceeds through the **b** pathway is a factor of $\times10^{6}$ higher ($7.38\times10^{-1}\ h^{-1}$). This large difference between the calculated TOFs, along with the data on deuterium scrambling, clearly indicates that the orientation of the ligands in the **b** pathway is consistent with the experimental results, whereas that in the **a** pathway is not. Moreover, the calculated TOF is close to the average experimental value of $8.00\times10^{-1}\ h^{-1}$, which lends further support to the conclusion that the **b** cycle is the dominant product-forming pathway in this reaction. The *trans* orientation of the hydrides in this route makes the species less stable and, consequently, more reactive.

For the **b** pathway, the ability to dissociate a molecule of phosphine was examined to explain the spectroscopic observations (see above). Calculations were performed for all of the intermediates (**5b–12b**) and revealed that one intermediate (**6b**) was more stable without a coordinated phosphine (Table 3).

Table 3. Energy of PCy_3 dissociation from intermediates **5b–12b**.

Compound	**5b**	**6b**	**7b**	**8b**	**9b**	**10b**	**11b**	**12b**
ΔG_{dissoc} [kJ mol^{-1}]	41.2	−6.4	29.4	61.1	63.7	16.0	43.8	15.7

However, the barrier for the addition of an amine to this species (without a coordinated phosphine) is 21.7 kJ mol^{-1} higher than that to species **6b**, which, in total, makes the pathway without phosphine 15.3 kJ mol^{-1} less favorable. Because species **6b** is located between two rate-limiting states, the concentration of this intermediate will have a strong influence on the overall rate of the reaction. This result correlates with the experimental observations, where the addition of phosphine shifts the equilibrium towards species **6b** and increases the overall rate, but the order of the reaction with respect to phosphine is less than one because some phosphine dissociates off. In addition, the doublet in the ^1H NMR spectrum at $\delta = -18.04$ ppm can be assigned to the dihydride species that is formed by PCy_3 dissociation from species **6b**.

Having determined the orientation of the ligands, the next step was to establish the geometrical details of the species that are involved in the catalytic cycle. All of the compounds in the catalytic cycle are 18-electron complexes, except for two intermediates, **5b** and **9b**, which both have an empty site and undergo β-hydride elimination. Notably, when molecular hydrogen has dissociated from species **12b** to form species **5b**, the alkoxide ligand changes its coordination from η^1 to η^3 by engaging in an agostic interaction between Ru and the α-C–H bond of the alkoxide. This interaction has also previously been observed in computational studies of the β-hydride elimination with alkoxides.[20] As shown in Figure 7, the Ru–H bond length changes from

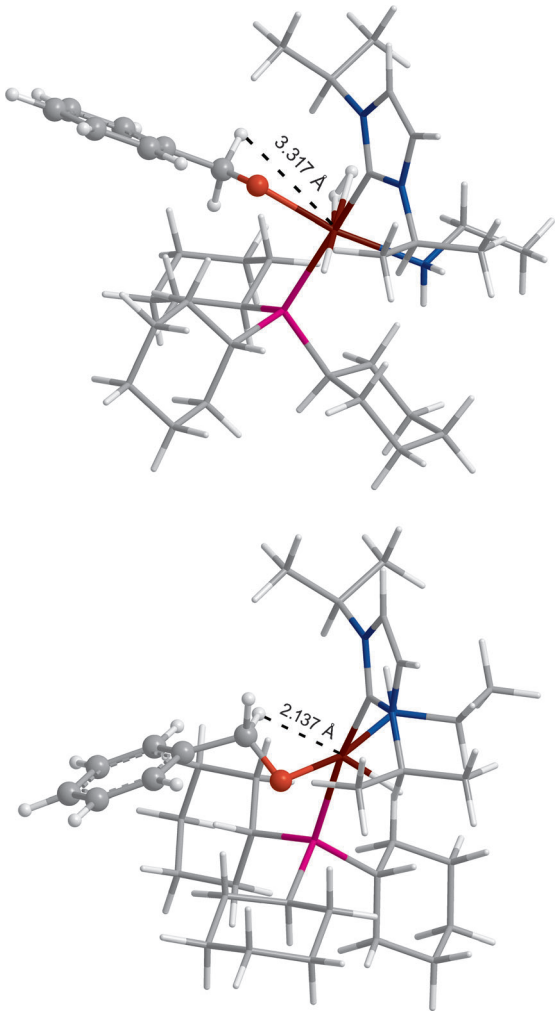

Figure 7. Calculated structures of compounds **12b** (top) and **5b** (bottom).

3.317 Å (**12b**) to 2.137 Å (**5b**). A similar agostic interaction is observed in the transformation from species **8b** into species **9b**. This result indicates that, during the catalytic cycle, ruthenium is electron poor and can be stabilized by receiving electron density from its ligands. This conclusion is also supported by experimental observations because amides are formed faster and in higher yields when electron-rich phosphines and NHCs, as well as benzyl alcohols, with electron-donating substituents in the *para* position are used (see above).

After the first β-hydride elimination, complex **6b** is formed. In this intermediate, the aldehyde acts as a η^2

ligand by binding to the ruthenium center through the π system of the C=O bond (Scheme 4). However, the geometry of the carbonyl carbon atom is close to that of an sp^3 hybri-

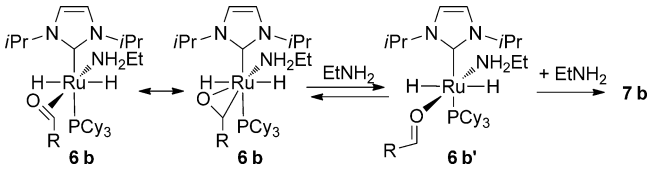

Scheme 4. Equilibrium between the isomers of compound **6b**.

dized carbon atom (out-of-plane angle for the C–H bond: 136°, $d_{C=O}=1.309$ Å), which implies that complex **6b** is more-correctly represented by a three-membered oxaruthinacycle (Figure 8). In the subsequent addition of the amine, complex **6b** rearranges into the aldehyde η^1 isomer (**6b′**; out-of-plane angle for the C–H bond: 169°, $d_{C=O}=1.235$ Å), which is then attacked by the amine to form species **7b** (Scheme 4).

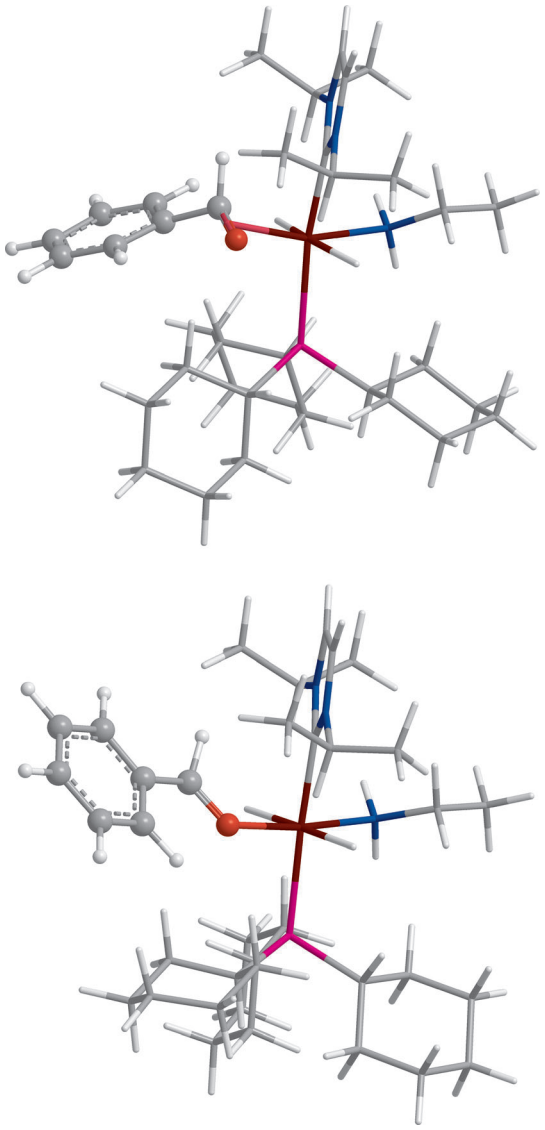

Figure 8. Calculated structures of compounds **6b** (top) and **6b′** (bottom).

The energetic parameters for the transformations **5b**→**6b** and **6b**→**7b** determine the overall rate of the reaction. These steps have approximately equal energy (E_a(**5b**–**TS1b**)=68.8 kJ mol^{-1}, E_a(**6b**–**TS2b**) = 68.7 kJ mol^{-1}) and, consequently, both steps should contribute equally to the limitations of the reaction. In the Hammett study, these two steps have opposite influence on the rate (and, hence, the ρ value) of the reaction. In the first step, electron-donating groups facilitate the β-hydride elimination, whereas, in the second step, they have the opposing effect in the nucleophilic addition to the aldehyde.

To model the Hammett study, the energy difference between the TDI and the TDTS was calculated for several benzyl alcohols with the following *para* substituents: NMe_2, OMe, SMe, Me, F, Cl, CF_3. Their relative reactivities were calculated by using Equation (2).

$$\lg\frac{k_X}{k_H}=\frac{\delta E_H-\delta E_X}{2.303RT},\ \delta E=E(\mathrm{TDTS})-E(\mathrm{TDI}) \qquad (2)$$

Different calculated energies were used in [Eq. (2)], but only the gas-phase energies and solution-phase energies showed good correlation with the σ^+ values (Figure 9).

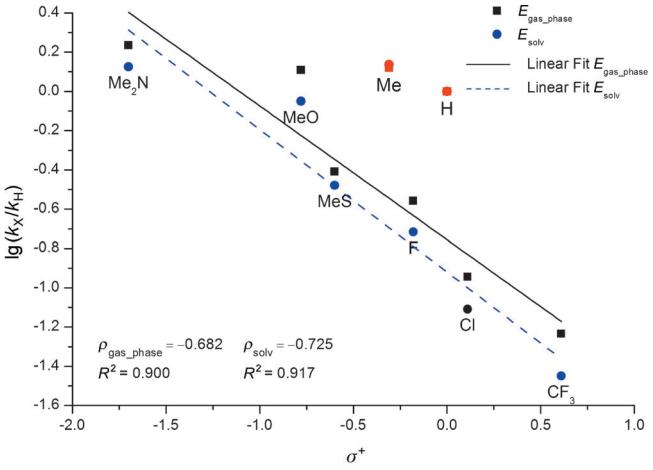

Figure 9. Hammett plot with calculated gas-phase and solvation energies (red points were excluded from the linear regression).

As can be seen from Figure 9, two substituents did not follow the overall good correlation; H and Me are both non-polar substituents and we ascribe the difference between these and the remaining polar substituents to inaccuracies in the solvation model. When examining the actual ρ values that were calculated by using the gas-phase energies ($\rho_{gas\,phase}=-0.68$) and the solution-phase energies ($\rho_{solv}=-0.73$), it is clear that the calculated slopes are somewhat higher than the experimental value ($\rho_{exp}=-0.15$). However, the calculated reactivity follows the same trend as the exper-

imental data, that is, that substrates with electron-donating substituents are more reactive than those with electron-withdrawing substituents.

The KIE for the reaction was also calculated by using the energetic-span model. In that case, the catalytic cycle with deuterated analogues had a δE value of 142.3 kJ mol^{-1}, which resulted in a TOF of $1.4\cdot10^{-2}$ h^{-1}. Thus, the KIE value was calculated as $KIE = TOF_H/TOF_D = 3.78$, which was significantly higher than that observed experimentally (KIE = 2.29). There may be several reasons for this discrepancy: First, benzyl alcohol was used in the computational model system whereas [D_{10}]-1-butanol was utilized in the experiment. This result indicates that the nature of the substituent on the α carbon atom of the alcohol does have a profound influence on the observed KIE value in the amidation reaction. Another way to calculate the KIE value is by using Equation (3).

$$KIE = \frac{k_H}{k_D} = e^{-\frac{\Delta G_a^H - \Delta G_a^D}{RT}}, \Delta G_a = \Delta G_{tot}(\mathbf{TS2b}) - \Delta G_{tot}(\mathbf{6b}) \qquad (3)$$

The KIE value for the system with EtOH was calculated to be 3.27, which is very close to the value obtained by using the energetic span model. This result shows that either of these two models may be used for the KIE calculations.

However, the KIE value from these calculations is still higher than the experimental value (2.29); the reason for this difference may partially lie in the experimental determination of the KIE. Commercially available [D_{10}]-1-butanol was used for the KIE experiments and it contained a small amount of C_4D_9OH. The amidation reaction was performed with 5% of PCy_3·HBF_4, which, after deprotonation with KO*t*Bu, would exchange hydrogen and deuterium with [D_{10}]-1-butanol. Presumably, 5–10% of C_4D_9OH was present in the experiment with [D_{10}]-1-butanol and this isotopic impurity would lower the value of the experimentally determined KIE.

Conclusion

The mechanism of the Ru–NHC-catalyzed amidation reaction between alcohols and amines was investigated by using experimental and theoretical methods. A Hammett study indicates that a small positive charge is built-up at the benzylic position in the transition state of the turnover-limiting step. The small value indicates that the rate of the reaction is not dominated by a single elementary reaction; instead, it is likely that two steps with opposite electronic character both influence the reaction rate.

The kinetic isotope effect was experimentally determined to be 2.29(±0.15), which suggests that breakage of the C–H bond is not the rate-limiting step, but that it is one of several slow steps in the catalytic cycle. These experimental results were further supported by the characterization of a plausible catalytic cycle by using DFT/M06 calculations. Both *cis*-dihydride and *trans*-dihydride intermediates were considered, but when the theoretical turnover frequencies (TOFs) were derived directly from the calculated DFT/M06 energies, we found that only the *trans*-dihydride pathway (Scheme 3, cycle **b**) was in agreement with the experimentally determined TOFs. The overall good agreement between the experimental and theoretical data illustrates that modern theoretical methods have matured to a point where their results can be used to predict and rationalize experimental observations. This result opens up the possibility for a number of new applications, such as in silico ligand screening, which is currently underway in our laboratory.

Computational Details

All calculations were performed with Jaguar[21] (version 7.8, release 109) by using the M06[22] or B3LYP functionals[23] in combination with the LACVP* basis set.[24] During our initial investigations, it became clear that the B3LYP functional did not adequately describe the non-bonded interactions that were responsible for discriminating between the possible reaction pathways; this deficiency of the B3LYP functional is well-known and the problem has been addressed previously by either appending a classic dispersion term[25] or by using a functional that incorporates terms for kinetic energy density.[26] Among the most-successful of these latter approaches are the M0x family of functionals reported by Truhlar and co-workers; herein, we chose the M06 functional, which has been optimized with a particular focus on organometallic systems and has been used successfully in an earlier study.[27]

All of the structures were optimized in the gas phase and the single-point solvation energy was calculated for the optimized structures by using a standard Poisson–Boltzmann solver with suitable parameters for benzene as the solvent (dielectric constant: $\varepsilon = 2.284$, probe radius: $r = 2.600$ Å). Gibbs free energies were obtained from the vibrational-frequency calculations for the gas-phase geometries at 298 K and 383 K. All of the transition states were characterized by the presence of one negative vibrational frequency.

Acknowledgements

We thank the Danish Council for Independent Research–Technology and Production Sciences (DFF) for financial support.

[1] a) V. R. Pattabiraman, J. W. Bode, *Nature* **2011**, *480*, 471–479; b) C. L. Allen, J. M. J. Williams, *Chem. Soc. Rev.* **2011**, *40*, 3405–3415; c) C. Chen, S. H. Hong, *Org. Biomol. Chem.* **2011**, *9*, 20–26.

[2] B. Shen, D. M. Makley, J. N. Johnston, *Nature* **2010**, *465*, 1027–1032.

[3] J. W. Bode, R. M. Fox, K. D. Baucom, *Angew. Chem.* **2006**, *118*, 1270–1274; *Angew. Chem. Int. Ed.* **2006**, *45*, 1248–1252.

[4] a) J.-F. Soulé, H. Miyamura, S. Kobayashi, *J. Am. Chem. Soc.* **2011**, *133*, 18550–18553; b) Y. Wang, D. Zhu, L. Tang, S. Wang, Z. Wang, *Angew. Chem.* **2011**, *123*, 9079–9083; *Angew. Chem. Int. Ed.* **2011**, *50*, 8917–8921.

[5] a) C. Gunanathan, Y. Ben-David, D. Milstein, *Science* **2007**, *317*, 790–792; b) L. U. Nordstrøm, H. Vogt, R. Madsen, *J. Am. Chem. Soc.* **2008**, *130*, 17672–17673; c) A. Prades, E. Peris, M. Albrecht, *Organometallics* **2011**, *30*, 1162–1167; d) N. D. Schley, G. E. Dobereiner, R. H. Crabtree, *Organometallics* **2011**, *30*, 4174–4179; e) K. Shimizu, K. Ohshima, A. Satsuma, *Chem. Eur. J.* **2009**, *15*, 9977–9980; f) J. Zhu, Y. Zhang, F. Shi, Y. Deng, *Tetrahedron Lett.* **2012**, *53*, 3178–3180.

[6] a) T. Zweifel, J.-V. Naubron, H. Grützmacher, *Angew. Chem.* **2009**, *121*, 567–571; *Angew. Chem. Int. Ed.* **2009**, *48*, 559–563; b) A. J. A.

Watson, A. C. Maxwell, J. M. J. Williams, *Org. Lett.* **2009**, *11*, 2667–2670.
[7] a) J. P. Shackleford, B. Shen, J. N. Johnston, *Proc. Natl. Acad. Sci. USA* **2012**, *109*, 44–46; b) I. Pusterla, J. W. Bode, *Angew. Chem.* **2012**, *124*, 528–531; *Angew. Chem. Int. Ed.* **2012**, *51*, 513–516.
[8] M. Montag, J. Zhang, D. Milstein, *J. Am. Chem. Soc.* **2012**, *134*, 10325–10328.
[9] a) G. Zeng, S. Li, *Inorg. Chem.* **2011**, *50*, 10572–10580; b) H. Li, X. Wang, F. Huang, G. Lu, J. Jiang, Z. Wang, *Organometallics* **2011**, *30*, 5233–5247; c) A. Nova, D. Balcells, N. D. Schley, G. E. Dobereiner, R. H. Crabtree, O. Eisenstein, *Organometallics* **2010**, *29*, 6548–6558.
[10] a) A. Maggi, R. Madsen, *Organometallics* **2012**, *31*, 451–455; b) C. Chen, Y. Zhang, S. H. Hong, *J. Org. Chem.* **2011**, *76*, 10005–10010; c) A. Sølvhøj, R. Madsen, *Organometallics* **2011**, *30*, 6044–6048; d) J. Zhang, M. Senthilkumar, S. C. Ghosh, S. H. Hong, *Angew. Chem.* **2010**, *122*, 6535–6539; *Angew. Chem. Int. Ed.* **2010**, *49*, 6391–6395; e) J. H. Dam, G. Osztrovszky, L. U. Nordstrøm, R. Madsen, *Chem. Eur. J.* **2010**, *16*, 6820–6827; f) S. C. Ghosh, S. H. Hong, *Eur. J. Org. Chem.* **2010**, 4266–4270; g) S. Muthaiah, S. C. Ghosh, J.-E. Jee, C. Chen, J. Zhang, S. H. Hong, *J. Org. Chem.* **2010**, *75*, 3002–3006; h) Y. Zhang, C. Chen, S. C. Ghosh, Y. Li, S. H. Hong, *Organometallics* **2010**, *29*, 1374–1378; j) S. C. Ghosh, S. Muthaiah, Y. Zhang, X. Xu, S. H. Hong, *Adv. Synth. Catal.* **2009**, *351*, 2643–2649.
[11] M. R. Netherton, G. C. Fu, *Org. Lett.* **2001**, *3*, 4295–4298.
[12] a) P. Fristrup, M. Tursky, R. Madsen, *Org. Biomol. Chem.* **2012**, *10*, 2569–2577; b) P. Fristrup, M. Kreis, A. Palmelund, P.-O. Norrby, R. Madsen, *J. Am. Chem. Soc.* **2008**, *130*, 5206–5215; c) J. H. Dam, P. Fristrup, R. Madsen, *J. Org. Chem.* **2008**, *73*, 3228–3235; d) P. Fristrup, L. B. Johansen, C. H. Christensen, *Chem. Commun.* **2008**, 2750–2752.
[13] a) C. Hansch, H. Gao, *Chem. Rev.* **1997**, *97*, 2995–3059; b) C. Hansch, A. Leo, R. W. Taft, *Chem. Rev.* **1991**, *91*, 165–195; c) X. Creary, M. E. Mehrsheikh-Mohammadi, S. McDonald, *J. Org. Chem.* **1987**, *52*, 3254–3263.
[14] D. H. Wertz, *J. Am. Chem. Soc.* **1980**, *102*, 5316–5322.
[15] J. K. C. Lau, D. V. Deubel, *J. Chem. Theory Comput.* **2006**, *2*, 103–106.
[16] a) E. Solari, S. Gauthier, R. Scopelliti, K. Severin, *Organometallics* **2009**, *28*, 4519–4526; b) A. Aranyos, G. Csjernyik, K. J. Szabó, J.-E. Bäckvall, *Chem. Commun.* **1999**, 351–352.
[17] C. Amatore, A. Jutand, *J. Organomet. Chem.* **1999**, *576*, 254–278.
[18] S. Kozuch, S. Shaik, *Acc. Chem. Res.* **2011**, *44*, 101–110.
[19] a) A. Uhe, S. Kozuch, S. Shaik, *J. Comput. Chem.* **2011**, *32*, 978–985; b) S. Kozuch, S. Shaik, *J. Phys. Chem. A* **2008**, *112*, 6032–6041; c) S. Kozuch, S. Shaik, *J. Am. Chem. Soc.* **2006**, *128*, 3355–3365.
[20] N. Sieffert, M. Bühl, *J. Am. Chem. Soc.* **2010**, *132*, 8056–8070.
[21] Jaguar, Version 7.8, Schrodinger, LLC, New York, NY, **2010**.
[22] Y. Zhao, D. G. Truhlar, *Theor. Chem. Acc.* **2008**, *120*, 215–241.
[23] a) A. D. Becke, *J. Chem. Phys.* **1993**, *98*, 5648–5652; b) C. Lee, W. Yang, R. G. Parr, *Phys. Rev. B* **1988**, *37*, 785–789.
[24] P. J. Hay, W. R. Wadt, *J. Chem. Phys.* **1985**, *82*, 270–283.
[25] a) S. Grimme, *J. Comput. Chem.* **2004**, *25*, 1463–1473; b) M. Elstner, P. Hobza, T. Frauenheim, S. Suhai, E. Kaxiras, *J. Chem. Phys.* **2001**, *114*, 5149–5155.
[26] a) B. B. Averkiev, Y. Zhao, D. G. Truhlar, *J. Mol. Catal. A* **2010**, *324*, 80–88; b) Y. Zhao, D. G. Truhlar, *Acc. Chem. Res.* **2008**, *41*, 157–167.
[27] X. Bantreil, G. Prestat, A. Moreno, D. Madec, P. Fristrup, P.-O. Norrby, P. S. Pregosin, G. Poli, *Chem. Eur. J.* **2011**, *17*, 2885–2896.

Received: July 5, 2012
Published online: October 15, 2012

